Received: 10 May 2019 | Revised: 9 July 2019 | Accepted: 9 July 2019

DOI: 10.1111/jace.16695

ORIGINAL ARTICLE

Journal of the American Ceramic Society

Correlative models for perovskites with rock salt B-site ordering

Evan Smith | **Claire Adams** | **Rick Ubic**

Micron School of Materials Science & Engineering, Boise State University, Boise, ID, USA

Correspondence
Rick Ubic, Micron School of Materials Science & Engineering, Boise State University, 1910 University Drive, Boise, ID 83725, USA.
Email: rickubic@boisestate.edu

Funding information
Micron School of Materials Science and Engineering at Boise State University

Abstract

Empirically derived predictive models describing synthesis-structure relationships have the potential to significantly improve and guide future research in a more cost-effective and timely manner; however, few of these models exist for cation ordering in perovskites. In this study, four compositions within the $AZn_{0.5}Ti_{0.5}O_3$ system (A = Nd, Sm, $Nd_{0.5}La_{0.5}$, $Nd_{0.5}Gd_{0.5}$) were synthesized using a conventional solid-state mixed-oxide method. X-ray diffraction data show evidence of long-range 1:1 rock salt cation ordering on the B site for all compositions. Additional data for other rock salt B-site ordered compositions were mined from literature. Correlative models for the B-site shrinkage (Δr_B) have been derived for each B-site ordered system, and a general model has been developed for rock salt B-site ordering from these specific models. This general model allows for the prediction of the room-temperature volume shrinkage resulting from rock salt B-site ordering using only published ionic radii data.

KEYWORDS

electroceramics, modeling/model, perovskites, titanates, X-ray methods

1 | INTRODUCTION

Predictive models for composition-structure-property relationships are essential to realizing the full potential of electroceramic materials. Ceramics with the perovskite structure possess a wider range of properties (eg, pyroelectricity, ferroelectricity, piezoelectricity, superconductivity, etc.) than ceramics with almost any other type of crystal structure;[1] thus, eliminating the need for expensive trial-and-error experiments by instead using predictive models to predict structures and properties is key to the future of the electroceramics industry.

There are a vast number of structural distortions in perovskites which cause deviations from the aristotypical perovskite structure in cubic space group $Pm\bar{3}m$. These structural distortions, such as cation ordering, can have significant implications for the materials properties, such as ionic conduction. In perovskites, cation ordering often occurs on alternating {001}, {110}, or {111} pseudocubic planes for both A-site substituted $A'_{0.5}A''_{0.5}BX_3$ or B-site substituted $AB'_{0.5}B''_{0.5}X_3$ complex perovskites.[2] Ordering on {111} (rock salt ordering) is typically preferred for B-site ordering, whereas {001} ordering (layered ordering) tends to be preferred for A-site ordering.

In 1980, Setter and Cross[3] were the first to study cation size and charge effects on the degree of ordering in $A(B'B'')O_3$ perovskites. According to their study, large differences in either charge or size of B′ and B″ ions tend to lead to a higher degree of cation ordering. Over the next couple of decades, these findings were seemingly corroborated by many studies.[4–7] In particular, Woodward et al[6] observed that if the B′ and B″ cations have a charge difference larger than two, then they will tend to form highly ordered structures; however, if the charge difference is equal to or less than two, then various degrees of ordering among the B cations will exist.

Interestingly, the large majority of rock salt B-site ordered perovskite oxides seem to prefer monoclinic symmetry in space group $P2_1/n$, with the second most preferential symmetry being cubic $Fm\bar{3}m$;[7–9] however, Howard et al[9] note that many of the perovskites listed with $P2_1/n$ symmetry may

actually have higher symmetry, and many of the perovskites listed with $Fm\bar{3}m$ symmetry may have lower symmetry due to varying degrees of octahedral tilting. This discrepancy is primarily due to the fact that the majority of the B-site ordered perovskites reported to date have been studied using X-ray diffraction, but octahedral tilting is notoriously difficult to detect via X-ray diffraction. It is typically visible via electron diffraction, but neutron diffraction would most likely be necessary to accurately quantify the degree of octahedral tilting in such cases.

The (Ca,Sr,Pb,Ba)$(Mg_{1/2}W_{1/2})O_3$ perovskite systems lend themselves particularly well to the study of B-site ordering due to the fact that they are reported[10–25] to exhibit long-range rock salt type ordering of Mg^{2+} and W^{6+} cations on the B site. The $CaMg_{1/2}W_{1/2}O_3$ (CMW) composition has been studied[10,11] via neutron and X-ray diffraction (XRD) and has been reported to exist in monoclinic space group $P2_1/n$. The low symmetry was attributed[10] to tilting of the BO_6 octahedra and an antiparallel shift of the A-site cations along the monoclinic [010]. Moreover, the $SrMg_{1/2}W_{1/2}O_3$ perovskite has been investigated[12–16] via neutron diffraction and XRD, and it has been reported with tetragonal symmetry in space group $I4/m$. Likewise, $BaMg_{1/2}W_{1/2}O_3$ has been studied[16–20] using neutron diffraction and XRD, but it has been reported with cubic symmetry in space group $Fm\bar{3}m$. In addition, the well-studied $PbMg_{1/2}W_{1/2}O_3$ (PMW) composition was initially reported[21] in cubic space group $Pm\bar{3}m$ but was later reported[22] with orthorhombic symmetry in space group $Pmmm$. Several more studies[23,24] seem to verify that PMW exhibits orthorhombic symmetry at room temperature, but in space group $Pmcn$; however, the most recent study[25] performed on PMW suggests that it crystalizes in cubic space group $Fm\bar{3}m$ at room temperature but transitions to orthorhombic space group $Pmcn$ below 8°C.

The $A^{3+}Zn_{0.5}Ti_{0.5}O_3$ perovskite system is an important system for many dielectric applications,[26–28] and it seems to readily display[26–29] long range rock salt B-site ordering. Ubic et al[26] reported a monoclinic symmetry in space group $P2_1/n$ for $LaZn_{0.5}Ti_{0.5}O_3$ (LZT) and observed a completely ordered B site via neutron diffraction. A seemingly different result was later observed by Aguadero et al,[29] who also used neutron diffraction but observed about 10% disorder on the B site; however, the difference is reconcilable considering the difference in experimental processes between the two studies. Aguadero et al[29] used soft-chemistry processing procedures and annealed their samples at 1150°C, whereas Ubic et al[26] used solid-state processing procedures and annealed their samples at 1400°C. The dielectric properties reported by Ubic et al[26] at 4.25 GHz were $\varepsilon_r = 34$, $Qf = 36\,090$ GHz, and $\tau_f = -70$ MK^{-1}.

$NdZn_{0.5}Ti_{0.5}O_3$ has been reported[27] to exist with monoclinic symmetry with a fully ordered B site. The following dielectric properties were also reported[27] at 8.5 GHz: $\varepsilon_r = 31.6$, $Qf = 170\,000$ GHz, and $\tau_f = -42$ ppm/°C. Additionally, $PrZn_{0.5}Ti_{0.5}O_3$ (PZT) and $GdZn_{0.5}Ti_{0.5}O_3$ (GZT) were studied[28] via X-ray and electron diffraction. Both compounds were observed[28] with monoclinic symmetry in space group $P2_1/n$, but GZT was reported with a fully ordered B site while PZT was reported with a 95% ordered B site. The B-site ordering was attributed to a large charge and size difference between the B-site cations (Zn^{2+} and Ti^{4+}). The following dielectric properties were also observed[28] at 1 MHz: $\varepsilon_r = 27$ & $\tan\delta = 0.003$ for PZT, and $\varepsilon_r = 17$ & $\tan\delta = 0.005$ for GZT.

Interestingly, $BiZn_{0.5}Ti_{0.5}O_3$ (BZT) was studied[30] using X-ray and electron diffraction and was reported[30] to exist with a completely disordered arrangement of Zn^{2+} and Ti^{4+} cations on the B site, which would seem to contradict the conclusions of Woodward et al.[6] Room temperature dielectric properties of $\varepsilon_r = 250$ and $\tan\delta = 0.1$ were observed[30] at 1 MHz.

$AR_{0.5}Ir_{0.5}O_6$ (A = Sr, Ba; R = Sc, Y, La, Lu)[31] and $SrCu_{0.5}Ir_{0.5}O_3$[32] perovskites were studied via X-ray diffraction and were all determined to exhibit a fully ordered B site. All of these compounds are reported with monoclinic symmetry except for $SrCu_{0.5}Ir_{0.5}O_3$, which was reported with tetragonal symmetry in space group $I4/m$. Moreover, these perovskites were observed to exhibit paramagnetic properties down to 4.5 K, and $SrCu_{0.5}Ir_{0.5}O_3$ was observed to exhibit magnetic properties above 15 K.

$SrY_{0.5}Ta_{0.5}O_3$[33,34] and $SrY_{0.5}Nb_{0.5}O_3$[33] were both studied via X-ray diffraction and they were observed with a fully ordered B site in monoclinic space group $P2_1/n$. $BaLn_{0.5}Nb_{0.5}O_3$ (Ln = Y, La, Pr, Nd, Sm, Eu, Gd, Tb, Dy, Ho, Er, Tm, Yb, Lu),[35] $BaLn_{0.5}Ta_{0.5}O_3$ (Ln = Y, all lanthanide species),[36] $SrLn_{0.5}Ta_{0.5}O_3$ (Ln = Nd, Pm, Sm, Eu, Gd, Tb, Dy, Ho, Er, Tm, Yb, Lu),[37] and $AIn_{0.5}Nb_{0.5}O_3$ (A = Ca, Sr, Ba)[38] perovskites were all studied using X-ray diffraction[35–37] or neutron diffraction.[38] All compositions were observed in monoclinic space group $P2_1/n$, except for members of the Ln = Dy-Lu series of the $BaLn_{0.5}Ta_{0.5}O_3$ system, which were reported in cubic space group $Fm\bar{3}m$. All compositions were also reported with long-range rock salt ordering on the B site. In addition, all of the compositions, except for the $AIn_{0.5}Nb_{0.5}O_3$ system, were reported with paramagnetic properties down to 5 K.

Interestingly compounds in the $SrM_{0.5}Mo_{0.5}O_3$ (M = Mg, Mn, Fe, Co, Ni, Zn)[39] system were determined via X-ray diffraction to exhibit triclinic symmetry in space group $P\bar{1}$ with nearly fully ordered B sites; however, the similar $SrCa_{0.5}Mo_{0.5}O_3$ perovskite compound has been studied[40] via neutron diffraction and was also reported[40] with a fully ordered B site but in monoclinic space group $P2_1/n$.

In 1926, Goldschmidt[41] introduced the perovskite tolerance factor, t_0, defined as follows:

$$t_0 = \frac{(r_A + r_X)}{\sqrt{2}\,(r_B + r_X)} \quad (1)$$

where r_A, r_B, and r_X are the ionic radii of A, B, and X ions, respectively.[42] Experimental parameters can be used to define the experimental pseudocubic lattice constant as follows:

$$a_{pc(Exptl.)} = \left(\frac{V}{Z}\right)^{1/3} \quad (2)$$

where V is the unit-cell volume and Z is the number of ABX_3 formula units per unit cell. By studying the $(A_{1-3x}Ln_{2x})TiO_3$ (A = Ca, Sr, Pb, Ba; Ln = La, Ce, Nd, Y) systems, an empirical model, which accounts for A-site vacancies among other extrinsic defects, has been recently developed[43–49] and effectively predicts pseudocubic lattice constants. The pseudocubic lattice constant, a_{pc}, can be defined in two ways according to this model:

$$a'_{pc} = \sqrt{2}\left(r_A + r_X\right) \quad (3)$$

$$a''_{pc} = 2\left(r_B + r_X\right) \quad (4)$$

The keys to this model are the concepts that the effective r_X is a function of t_0 and that the effective r_A is a function of both x and t_0, which can now be redefined[43] as the ratio of Equations (3) and (4):

$$t_0 = \frac{a'_{pc}}{a''_{pc}} = \frac{\left(r_A + r_X\right)}{\sqrt{2}\left(r_B + r_X\right)} \quad (5)$$

Ubic et al[43,46–48] have also derived a revised method for determining the perovskite tolerance factor, which accounts for a variety of extrinsic defects:

$$t' = \frac{a_{pc} - 0.011730139}{0.7209203\left(r_B + r_X\right)} - 1.760998, \quad (6)$$

where a_{pc} is determined either experimentally or from an empirical model.[49] One of the major advantages of using t' is that the ambiguity in determining effective sizes of partially-occupied A sites is eliminated. It also does not require foreknowledge of r_A, which is not always known, and is far better than t_0 (Equation 1) at predicting octahedral distortions. In addition, Equation 6 can be solved for a_{pc} as:

$$a_{pc} = 0.7209203\left(t' + 1.760998\right)\left(r_B + r_X\right) + 0.011730139, \quad (7)$$

which yields yet a third way to define a_{pc}, where t' is determined from values of r_A and t_0 using a correlative model.[49]

It has recently been established[50–52] that, while layered A-site ordering results in a counterintuitive unit-cell volume *increase* compared to the disordered structure, rock salt B-site ordering results in the expected unit-cell volume *decrease* compared to the disordered structure. This result was explained crystalochemically[50] by the fact that ordering causes more efficient packing in perovskites *within* ordered planes but an expansion of bonds *perpendicular* to them. In other words, bonds which lie in or near the ordering planes will contract whereas those more perpendicular will tend to expand. For this reason, a strong indicator of rock salt B-site ordering within this model[51] is an overestimation of B-X bond length, which results in large positive errors (1%-3%) in both a'_{pc} and a''_{pc}. In these cases, a negative Δr_B correction term can be introduced to effectively correct for these errors.

In this work, four compositions within the $A(Zn_{0.5}Ti_{0.5})O_3$ (A = Nd, Sm, $Nd_{0.5}La_{0.5}$, and $Nd_{0.5}Gd_{0.5}$) (NZT, SZT, NLZT, and NGZT) perovskite system were produced. Another 38 rock salt B-site ordered perovskites were also mined from

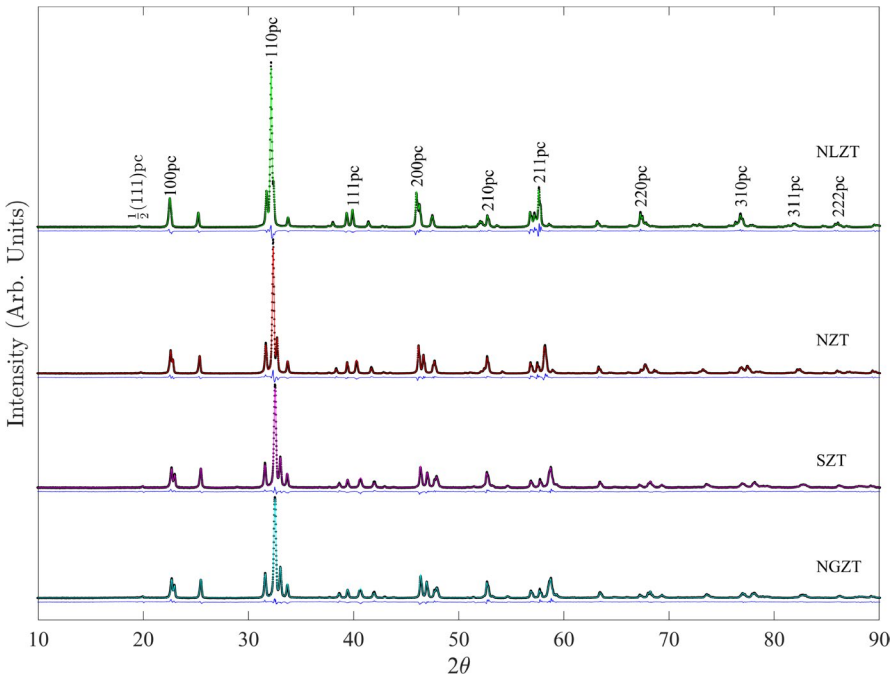

FIGURE 1 Rietveld plots of NLZT, NZT, SZT, and NGZT. The data points correspond to the observed intensities. Both refinement results and difference patterns are shown for each composition, and all peaks are indexed according to the pseudocubic unit cell

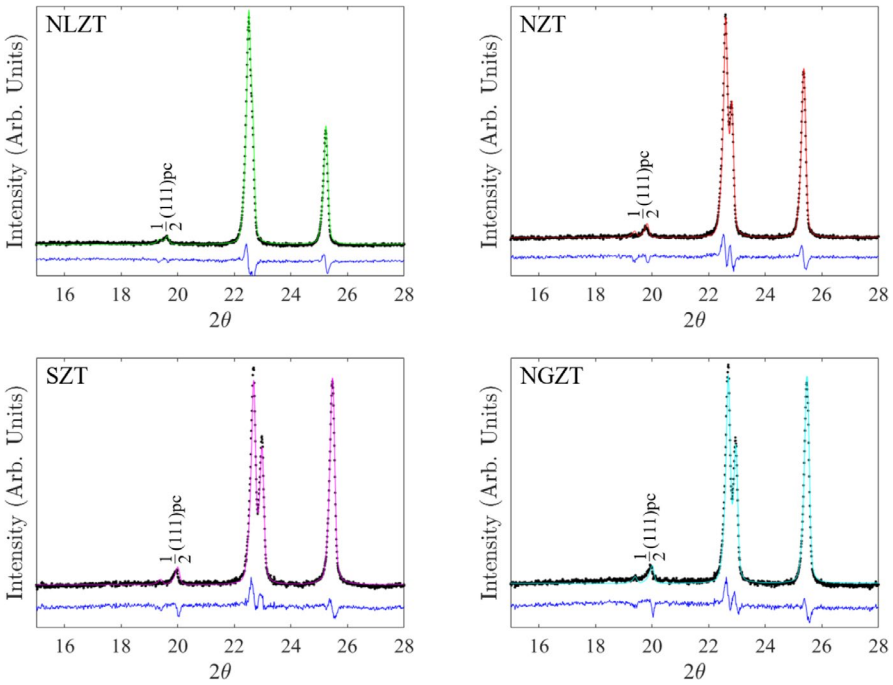

FIGURE 2 Rietveld plots of NLZT, NZT, SZT, and NGZT in the range $15° \leq 2\theta \leq 28°$ showing the ½(111)pc peak fit

literature. Empirical models were derived for each specific B-site ordered system. From these data, a general empirical model has been derived for the B-site size correction factor, Δr_B, similar to the A-site model recently derived by Smith et al.[52]

2 | MATERIALS AND METHODS

Four compositions in the system $A(Zn_{0.5}Ti_{0.5})O_3$ (A = Nd, Sm, $Nd_{0.5}La_{0.5}$, $Nd_{0.5}Gd_{0.5}$) were synthesized via the solid-state mixed-oxide route. As-received La_2O_3 (99.9%, Acros Organics, Fair Lawn, NJ), Nd_2O_3 (99%, Alfa-Aesar, Ward Hill, MA), and Sm_2O_3 (99.9%, Alfa-Aesar, Ward Hill, MA) powders were first hydroxylated by mixing with an excess of deionized water and drying overnight, forming $La(OH)_3$, $Nd(OH)_3$, or $Sm(OH)_3$. Stoichiometric amounts of ZnO (99.9%, Alfa-Aesar, Ward Hill, MA), TiO_2 (99.5%, Alfa-Aesar, Ward Hill, MA), Gd_2O_3 (99.9%, Alfa-Aesar, Ward Hill, MA) $La(OH)_3$, $Nd(OH)_3$, and $Sm(OH)_3$ were then ball-milled with yttria-stabilized ZrO_2 (YSZ) media using deionized water in a high-density nylon pot for ~6 hours. Powders were then dried overnight in an atmospheric drying oven at ~98°C until all the water was evaporated. An initial dehydroxylation heat treatment was conducted in an open crucible at 600°C for 2 hours. Calcination was subsequently conducted in a closed crucible for two hours in a box furnace (1807FL, CM Furnaces Inc., Bloomfield, NJ) at 1200°C. After calcination, the powders were ground using a porcelain mortar and pestle. Powders were then re-calcined in a closed crucible for two hours at 1400°C, after which they were ball-milled again with YSZ media using deionized water in a high-density nylon pot for ~24 hours. The mixture was then dried overnight in an atmospheric drying oven at ~98°C until all the water had evaporated. The mixture was then ground again using a mortar and pestle and finally sieved to under 250 μm.

Powder XRD measurements were performed in a diffractometer (Miniflex-600, Rigaku, Woodlands, TX) operating with convergent-beam geometry and CuK_α radiation.

TABLE 1 Refinement results for zinc titanates

A-site species	$(Nd_{0.5}La_{0.5})$	Nd	Sm	$(Nd_{0.5}Gd_{0.5})$
a (Å)	7.84135(8)	7.78132(7)	7.72469(9)	7.73249(9)
b (Å)	5.63482(5)	5.64713(4)	5.65861(6)	5.65563(6)
c (Å)	5.52172(5)	5.46671(5)	5.41550(7)	5.41560(6)
β (°)	90.021(4)	90.099(1)	90.184(1)	90.211(1)
x (4(*e*) A-site)	0.2510(3)	0.2504(4)	0.2500(3)	0.2505(3)
y (4(*e*) A-site)	0.0456(1)	0.0535(1)	0.0602(1)	0.0593(1)
z (4(*e*) A-site)	0.9895(2)	0.9876(2)	0.9851(2)	0.9851(2)
wR%	7.81	5.78	3.58	3.71

TABLE 2 Experimental and calculated pseudocubic lattice constants (Å) for 42 rock salt B-site ordered perovskites[11,13,18,25,26,28,31–40,53–65]

ICSD #	Composition	$a_{pc(exptl.)}$ (Å)	a_{pc} Equation 7	Error%	a'_{pc} Equation 3	Error%	a''_{pc} Equation 4	Error%
172775	$La(Zn_{0.5}Ti_{0.5})O_3$	3.9503	3.9903	1.0114	3.9966	1.1701	3.9868	0.9240
251934	$Gd(Zn_{0.5}Ti_{0.5})O_3$	3.8755	3.9794	2.6795	4.0703	5.0255	3.9754	2.5763
251933	$Pr(Zn_{0.5}Ti_{0.5})O_3$	3.9264	3.9508	0.6226	3.9854	1.5034	3.9454	0.4845
[a]	$(Nd_{0.5}La_{0.5})(Zn_{0.5}Ti_{0.5})O_3$	3.9364	3.9646	0.7177	3.9861	1.2627	3.9599	0.5974
[a]	$Nd(Zn_{0.5}Ti_{0.5})O_3$	3.9161	3.9488	0.8370	3.9863	1.7937	3.9433	0.6960
[a]	$Sm(Zn_{0.5}Ti_{0.5})O_3$	3.8969	3.9447	1.2249	3.9930	2.4664	3.9389	1.0778
[a]	$(Nd_{0.5}Gd_{0.5})(Zn_{0.5}Ti_{0.5})O_3$	3.8976	3.9481	1.2953	4.0120	2.9363	3.9425	1.1527
155217	$Ca(Mg_{0.5}W_{0.5})O_3$	3.8741	3.9515	1.9985	3.9628	2.2903	3.9468	1.8781
151703	$Sr(Mg_{0.5}W_{0.5})O_3$	3.9570	4.0298	1.8398	4.0129	1.4134	4.0295	1.8335
262318	$Ba(Mg_{0.5}W_{0.5})O_3$	4.0542	4.1339	1.9660	4.1153	1.5055	4.1395	2.1047
262284	$Pb(Mg_{0.5}W_{0.5})O_3$	3.9996	4.0724	1.8213	4.0469	1.1834	4.0746	1.8753
170684	$Sr(Y_{0.5}Nb_{0.5})O_3$	4.1263	4.2362	2.6632	4.2257	2.4083	4.2360	2.6592
193235	$Sr(Yb_{0.5}Nb_{0.5})O_3$	4.1028	4.2050	2.4913	4.1931	2.2029	4.2047	2.4846
247459	$Sr(Y_{0.5}Ta_{0.5})O_3$	4.1237	4.2362	2.7286	4.2257	2.4735	4.2360	2.7246
88838	$Ba(Pr_{0.5}Nb_{0.5})O_3$	4.2878	4.4298	3.3114	4.3766	2.0707	4.4279	3.2687
95524	$Sr(Tm_{0.5}Ta_{0.5})O_3$	4.1117	4.2166	2.5532	4.2053	2.2772	4.2164	2.5475
172169	$Sr(In_{0.5}Nb_{0.5})O_3$	4.0568	4.1399	2.0498	4.1256	1.6973	4.1395	2.0389
290859	$Ba(La_{0.5}Ta_{0.5})O_3$	4.3198	4.4696	3.4688	4.4143	2.1878	4.4670	3.4087
88152	$Sr(Sc_{0.5}Ir_{0.5})O_3$	3.9917	4.0253	0.8413	4.0084	0.4177	4.0251	0.8358
88153	$Ba(Sc_{0.5}Ir_{0.5})O_3$	4.0738	4.1291	1.3574	4.1113	0.9214	4.1349	1.4991
88154	$Sr(Y_{0.5}Ir_{0.5})O_3$	4.0923	4.1684	1.8596	4.1551	1.5351	4.1680	1.8502
88155	$Ba(Y_{0.5}Ir_{0.5})O_3$	4.1745	4.2775	2.4674	4.2373	1.5063	4.2791	2.5063
88156	$Ba(La_{0.5}Ir_{0.5})O_3$	4.2836	4.4032	2.7915	4.3517	1.5892	4.4019	2.7514
88157	$Sr(Lu_{0.5}Ir_{0.5})O_3$	4.0642	4.1315	1.6551	4.1169	1.2963	4.1310	1.6439
88158	$Ba(Lu_{0.5}Ir_{0.5})O_3$	4.1461	4.2402	2.2691	4.2047	1.4123	4.2428	2.3316
192738	$Sr(Cu_{0.5}Ir_{0.5})O_3$	3.9471	3.9640	0.4263	3.9472	0.0027	3.9644	0.4372
246736	$Sr(Cr_{0.5}Sb_{0.5})O_3$	3.9328	3.9386	0.1475	3.9224	-0.2633	3.9395	0.1696
157007	$Sr(Ga_{0.5}Sb_{0.5})O_3$	3.9284	3.9428	0.3658	3.9265	-0.0486	3.9436	0.3857
33623	$Ba(Sc_{0.5}Sb_{0.5})O_3$	4.1015	4.1579	1.3746	4.1349	0.8140	4.1628	1.4942
246959	$Sr(Sm_{0.5}Sb_{0.5})O_3$	4.1607	4.2539	2.2409	4.2442	2.0066	4.2539	2.2385
247246	$Sr(In_{0.5}Sb_{0.5})O_3$	4.0508	4.1026	1.2788	4.0871	0.8971	4.1021	1.2672
262994	$Sr(Sc_{0.5}Sb_{0.5})O_3$	4.0172	4.0522	0.8728	4.0357	0.4600	4.0519	0.8637
50040	$Ba(Bi_{0.5}Sb_{0.5})O_3$	4.2750	4.4298	3.6205	4.3766	2.3761	4.4279	3.5777
84660	$Ba(Tl_{0.5}Sb_{0.5})O_3$	4.1905	4.2918	2.4180	4.2501	1.4222	4.2930	2.4482
97487	$La(Li_{0.5}Ru_{0.5})O_3$	3.9364	3.9700	0.8536	3.9751	0.9845	3.9662	0.7567
90653	$Sr(Ho_{0.5}Ru_{0.5})O_3$	4.0833	4.1646	1.9913	4.1512	1.6627	4.1642	1.9817
93361	$Sr(Tb_{0.5}Ru_{0.5})O_3$	4.1019	4.1857	2.0419	4.1730	1.7344	4.1853	2.0337
153132	$Sr(Tb_{0.5}Ru_{0.5})O_3$	4.0976	4.1857	2.1484	4.1730	1.8406	4.1853	2.1402
380254	$Sr(Ca_{0.5}Mo_{0.5})O_3$	4.1010	4.2857	3.5056	4.2774	4.3023	4.2858	4.5061
247346	$Sr(Mg_{0.5}Mo_{0.5})O_3$	3.9501	4.0209	1.7929	4.0039	1.3640	4.0207	1.7882
247350	$Sr(Ni_{0.5}Mo_{0.5})O_3$	3.9323	3.9945	1.5792	3.9775	1.1469	3.9945	1.5803
247351	$Sr(Zn_{0.5}Mo_{0.5})O_3$	3.9627	4.0387	1.9193	4.0220	1.4960	4.0384	1.9117

[a]This work.

TABLE 3 42 rock salt B-site ordered perovskites accounting for cation effective sizes (Å)[11,13,18,25,26,28,31–40,53–65]

ICSD #	Composition	Δr_B	a_{pc} Equation 7	Error%	a'_{pc} Equation 3	Error%	a''_{pc} Equation 4	Error%
172775	$La(Zn_{0.5}Ti_{0.5})O_3$	−0.01977	3.9503	−0.0006	3.9544	0.1033	3.9461	−0.1062
251934	$Gd(Zn_{0.5}Ti_{0.5})O_3$	−0.04341	3.8501	−0.6558	3.9329	1.4816	3.8412	−0.8848
251933	$Pr(Zn_{0.5}Ti_{0.5})O_3$	−0.01416	3.9174	−0.2284	3.9498	0.5954	3.9109	−0.3939
[a]	$(Nd_{0.5}La_{0.5})(Zn_{0.5}Ti_{0.5})O_3$	−0.01500	3.9316	−0.1215	3.9509	0.3697	3.9259	−0.2645
[a]	$Nd(Zn_{0.5}Ti_{0.5})O_3$	−0.01773	3.9065	−0.2452	3.9411	0.6387	3.8995	−0.4222
[a]	$Sm(Zn_{0.5}Ti_{0.5})O_3$	−0.02397	3.8843	−0.3232	3.9287	0.8140	3.8764	−0.5263
[a]	$(Nd_{0.5}Gd_{0.5})(Zn_{0.5}Ti_{0.5})O_3$	−0.02527	3.8799	−0.4544	3.9394	1.0718	3.8717	−0.6627
155217	$Ca(Mg_{0.5}W_{0.5})O_3$	−0.03775	3.8738	−0.0058	3.8808	0.1732	3.8674	−0.1724
151703	$Sr(Mg_{0.5}W_{0.5})O_3$	−0.03852	3.9624	0.1360	3.9457	−0.2859	3.9628	0.1475
262318	$Ba(Mg_{0.5}W_{0.5})O_3$	−0.04279	4.0516	−0.0635	4.0504	−0.0937	4.0598	0.1396
262284	$Pb(Mg_{0.5}W_{0.5})O_3$	−0.03986	4.0052	0.1401	3.9835	−0.4030	4.0092	0.2401
170684	$Sr(Y_{0.5}Nb_{0.5})O_3$	−0.05453	4.1314	0.1239	4.1168	−0.2295	4.1310	0.1129
193235	$Sr(Yb_{0.5}Nb_{0.5})O_3$	−0.05100	4.1081	0.1305	4.0928	−0.2425	4.1076	0.1190
247459	$Sr(Y_{0.5}Ta_{0.5})O_3$	−0.05591	4.1288	0.1247	4.1142	−0.2310	4.1284	0.1136
88838	$Ba(Pr_{0.5}Nb_{0.5})O_3$	−0.06781	4.3007	0.3020	4.2580	−0.6935	4.3018	0.3264
95524	$Sr(Tm_{0.5}Ta_{0.5})O_3$	−0.05227	4.1169	0.1281	4.1019	−0.2377	4.1165	0.1168
172169	$Sr(In_{0.5}Nb_{0.5})O_3$	−0.04185	4.0625	0.1399	4.0461	−0.2644	4.0621	0.1300
290859	$Ba(La_{0.5}Ta_{0.5})O_3$	−0.07127	4.3342	0.3331	4.2882	−0.7315	4.3344	0.3387
88152	$Sr(Sc_{0.5}Ir_{0.5})O_3$	−0.01580	3.9974	0.1422	3.9804	−0.2838	3.9974	0.1425
88153	$Ba(Sc_{0.5}Ir_{0.5})O_3$	−0.02925	4.0729	−0.0226	4.0667	−0.1734	4.0804	0.1624
88154	$Sr(Y_{0.5}Ir_{0.5})O_3$	−0.03759	4.0978	0.1331	4.0822	−0.2479	4.0973	0.1217
88155	$Ba(Y_{0.5}Ir_{0.5})O_3$	−0.05043	4.1810	0.1571	4.1542	−0.4865	4.1853	0.2585
88156	$Ba(La_{0.5}Ir_{0.5})O_3$	−0.05611	4.2963	0.2977	4.2541	−0.6880	4.2975	0.3246
88157	$Sr(Lu_{0.5}Ir_{0.5})O_3$	−0.03330	4.0698	0.1387	4.0536	−0.2612	4.0694	0.1284
88158	$Ba(Lu_{0.5}Ir_{0.5})O_3$	−0.04671	4.1507	0.1116	4.1290	−0.4128	4.1559	0.2350
192738	$Sr(Cu_{0.5}Ir_{0.5})O_3$	−0.00677	3.9524	0.1330	3.9359	−0.2852	3.9530	0.1485
246736	$Sr(Cr_{0.5}Sb_{0.5})O_3$	−0.00047	3.9378	0.1275	3.9217	−0.2828	3.9387	0.1499
157007	$Sr(Ga_{0.5}Sb_{0.5})O_3$	−0.00559	3.9334	0.1256	3.9174	−0.2817	3.9343	0.1503
33623	$Ba(Sc_{0.5}Sb_{0.5})O_3$	−0.02868	4.1028	0.0319	4.0902	−0.2746	4.1094	0.1924
246959	$Sr(Sm_{0.5}Sb_{0.5})O_3$	−0.04558	4.1654	0.1129	4.1520	−0.2089	4.1650	0.1035
247246	$Sr(In_{0.5}Sb_{0.5})O_3$	−0.02517	4.0564	0.1407	4.0399	−0.2669	4.0561	0.1313
262994	$Sr(Sc_{0.5}Sb_{0.5})O_3$	−0.01635	4.0229	0.1432	4.0060	−0.2783	4.0227	0.1381
50040	$Ba(Bi_{0.5}Sb_{0.5})O_3$	−0.07484	4.2873	0.2885	4.2461	−0.6761	4.2887	0.3206
84660	$Ba(Tl_{0.5}Sb_{0.5})O_3$	−0.04904	4.1980	0.1811	4.1685	−0.5237	4.2018	0.2705
97487	$La(Li_{0.5}Ru_{0.5})O_3$	−0.01660	3.9367	0.0076	3.9401	0.0941	3.9323	−0.1045
90653	$Sr(Ho_{0.5}Ru_{0.5})O_3$	−0.04045	4.0888	0.1351	4.0730	−0.2524	4.0883	0.1239
93361	$Sr(Tb_{0.5}Ru_{0.5})O_3$	−0.04146	4.1073	0.1307	4.0919	−0.2430	4.1068	0.1193
153132	$Sr(Tb_{0.5}Ru_{0.5})O_3$	−0.04375	4.1030	0.1318	4.0876	−0.2452	4.1026	0.1203
380254	$Sr(Ca_{0.5}Mo_{0.5})O_3$	−0.09296	4.1063	0.1309	4.0910	−0.2435	4.1059	0.1195
247346	$Sr(Mg_{0.5}Mo_{0.5})O_3$	−0.03762	3.9554	0.1339	3.9388	−0.2855	3.9559	0.1482
247350	$Sr(Ni_{0.5}Mo_{0.5})O_3$	−0.03323	3.9374	0.1274	3.9212	−0.2827	3.9382	0.1500
247351	$Sr(Zn_{0.5}Mo_{0.5})O_3$	−0.04017	3.9681	0.1375	3.9513	−0.2861	3.9685	0.1468

[a]This work.

Rietveld refinements were performed on the XRD patterns using GSAS II (Los Alamos National Laboratory, NM). The background was fitted with a Debye diffuse scattering function with six terms. All compositions were refined in monoclinic space group $P2_1/n$ allowing the cation occupancies and the coordinates of the A-site species in the 4*e* sites to vary.

3 | RESULTS AND DISCUSSION

Figures 1 and 2 show the XRD patterns and refinement fits for each of the four compositions that were produced within the $A(Zn_{0.5}Ti_{0.5})O_3$ system, clearly showing that all the compositions had successfully been produced with complete phase purity. Figure 1 also shows that the 110 pseudocubic peak is split into a triplet, which is one of the characteristics of an orthorhombic distortion. This triplet arises due to slight differences in the spacings of the $(0\bar{1}1)_{pc}$, $\{110\}_{pc}/\{101\}_{pc}$, and $(011)_{pc}$; however, the structure is actually monoclinic in space group $P2_1/n$ due to the presence of long-range rock salt ordering of Zn^{2+} and Ti^{4+} cations on the B site.

The existence of $\frac{1}{2}\{odd,odd,odd\}_{pc}$ peaks may indicate 1:1 B-site ordering; however, $\frac{1}{2}\{odd,odd,odd\}_{pc}$ superlattice reflections are also commonly associated with anti-phase octahedral tilting, which makes it difficult to unambiguously identify the origin of these superlattice reflections via XRD alone; nevertheless, Rietveld analyses of the XRD patterns do suggest that all four of these perovskites exhibit fully ordered B sites.

Table 1 shows the results of the Rietveld refinements performed on each of the four compositions within the $A(Zn_{0.5}Ti_{0.5})O_3$ system. The refinements suggest that all four of these perovskites exhibit monoclinic symmetry in space group $P2_1/n$ and display full rock salt ordering of Zn^{2+} and Ti^{4+} cations on the B site. These results also suggest that the samples become increasingly monoclinic (ie, β increases) as the size of the A-site species decreases (ie, as the tolerance factor decreases)

Table 2 shows the errors in a'_{pc}, a''_{pc}, and a_{pc}, (Equations 3, 4, and 7) with respect to the experimental pseudocubic lattice constants. Table 3 shows the B-site size correction parameters and the resultant reduced errors in Equation 3, 4, and 7. The data from Table 2 shows that, in general, the model overestimates the pseudocubic lattice constant for rock salt B-site ordered perovskites, which supports the hypothesis[50] that shrinking bonds within ordered planes will dominate over the effects electrostatic repulsions pushing ordered planes apart

The large positive errors in pseudocubic lattice constants predicted from the uncorrected model (Table 2) result from an apparent overestimation of r_B. Somewhat predictably, the uncorrected model seems to be less accurate for compounds with large differences in B-site cation sizes, whereas it appears to be far more accurate for compounds with similar B-site cation sizes. For instance, the model produces an error of 4.506% when predicting a''_{pc} in $Sr(Ca_{0.5}Mo_{0.5})O_3$, in which the size difference between Ca^{2+} and Mo^{6+} ions is 0.41 Å; however, the model only produces a 0.170% error in a''_{pc} for $Sr(Cr_{0.5}Ir_{0.5})O_3$, in which the size difference between Cr^{3+} and Ir^{5+} ions is just 0.015 Å.

TABLE 4 Coefficients of Equation 8 and the goodness of fit, R^2

$r_{B,small}$	*A*	*B*	*C*	R^2
Nb, Ta	0.3858	−3.3406	7.1619	0.9809
Ir	0.3529	−3.0608	6.5796	0.9889
Sb	−0.1986	1.4324	−2.5646	0.9908
Ru	0.3707	−3.1345	6.5778	0.9922
Mo	−0.8958	6.8529	−13.1282	0.9999
MgW	−0.2328	1.8175	−3.5842	0.9970
ZnTi	−5.3117	41.6784	−81.7733	0.9836

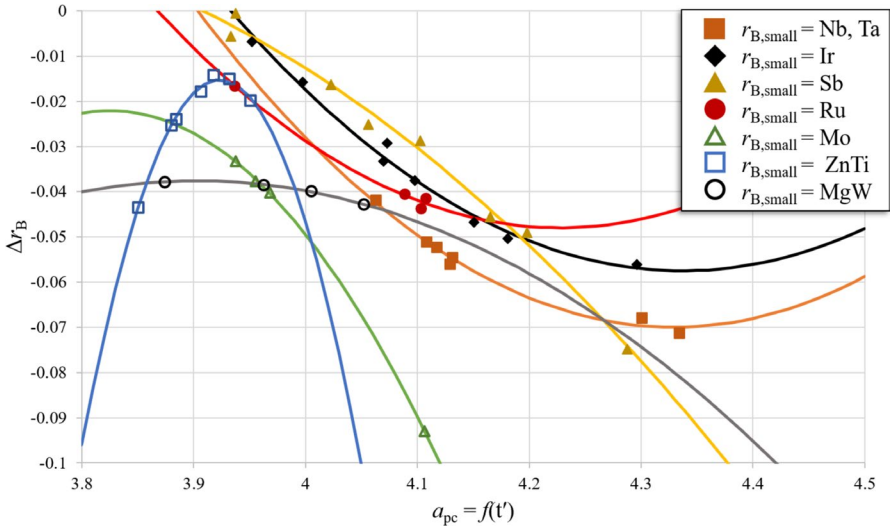

FIGURE 3 B-site size adjustment factors as functions of the pseudocubic lattice constant (Equation 7)

To effectively minimize and account for the errors coming from the volume contraction upon ordering, the values of r_B were decreased by an amount Δr_B. The value of Δr_B was determined by incrementally decreasing the value of r_B until the errors in a_{pc} (Equation 7), a'_{pc}(Equation 3), and a''_{pc} (Equation 4) were simultaneously minimized. It should be noted that a_{pc} and a''_{pc} are more sensitive to changes in B-site size than is a'_{pc} due to the fact that both a_{pc} and a''_{pc} depend directly on r_B. Thus, the errors in a'_{pc}(Equation 3) tend to be the largest in this case. Table 3 displays the results of this iterative process. Also, Equation 7 is used to calculate a_{pc} in Tables 2 and 3, where t' is determined from t_0 and r_A via an empirical model.[49] Additionally, Equations 3 and 4 are used to determine a'_{pc} and a''_{pc} in Tables 2 and 3, where the effective r_X is calculated from a correlative model[49] using t' and the Shannon radius of the X-site species.

It should be noted that all 42 compositions in Tables 2 and 3 were sorted into series based upon the smallest B-site cation in each, $r_{B,small}$, in order to develop a model for the B-site size adjustment factor with relation to the B-site size. This process created seven unique series of data (ie, compounds with Mo, Ru, Sb, Ir, Nb or Ta, $Mg_{½}W_{½}$, or $Zn_{½}Ti_{½}$ on the B site). A correlative model was then developed for each series.

The fact that Nb^{5+} and Ta^{5+} have the same charge and ionic size makes it impossible to isolate the effects of size and charge in compounds containing either of these species; however, compounds containing either Nb^{5+} or Ta^{5+} as the

TABLE 5 Coefficients of Equation (9) and the goodness of fit, R^2

Coefficient	*A*	*b*	*c*	R^2
A	−0.11987	0.80266	1.29757	0.9715
B	0.75396	−6.33299	−10.29258	0.9709
C	−1.12758	12.49349	20.42735	0.9701

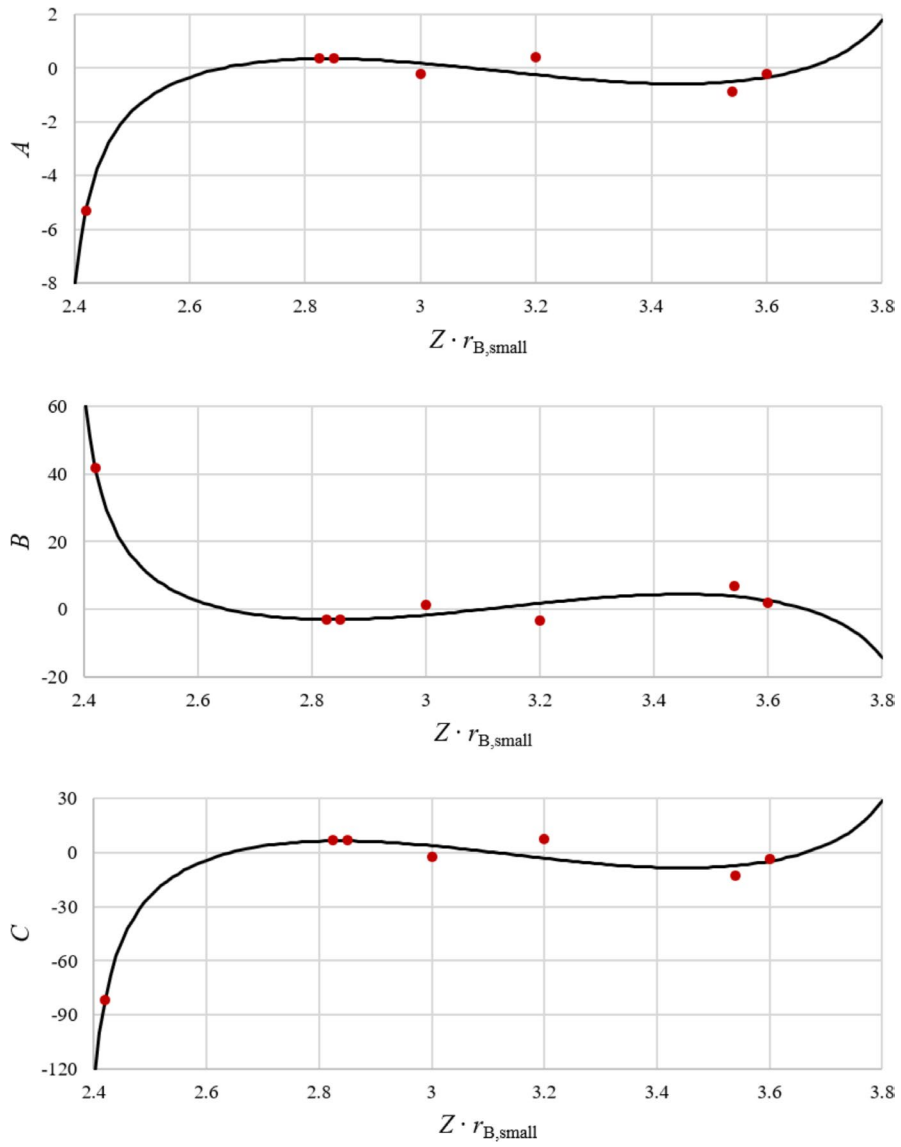

FIGURE 4 Coefficients of Equation 8 as a function of charge (Z) and ionic radius of the smallest B-site species, $r_{B,small}$

smallest B-site species produced very similar Δr_B vs a_{pc} curves. Despite the fact that Nb and Ta have very different atomic masses (m_{Nb} = 92.906 amu and m_{Ta} = 180.95 amu), it would appear that the model is only sensitive to size and charge differences between two species. Thus, it was possible to consider these compounds together in a single series.

Figure 3 shows the relationship between the B-site size correction factor, Δr_B, and pseudocubic lattice constant, a_{pc}. These curves demonstrate that the general trend is clearly a quadratic polynomial and can be represented generically by Equation 8:

$$\Delta r_B = Aa_{pc}^2 + Ba_{pc} + C, \quad (8)$$

where a_{pc} is calculated from Equation 7. Since Equation 7 predicts a_{pc} using solely ionic radii data,[42] Δr_B can be predicted only using ionic radii data[42] as well. The coefficients and goodness of fit for all seven of these curves are listed in Table 4.

Figure 4 shows the relationship between the coefficients of Equation 8 and the product of charge and size of the smallest B-site cation, $Z \bullet r_{B,small}$. Not only is this model sensitive to both the size and charge of B-site cations, but all three of the coefficients (A, B, and C) are related to the charge and size of the smallest B-site species in each composition by the same trigonometric function:

$$\text{Coeff} = a + b\tan\left(2Zr_{B,small}\right) + c\sin\left(3Zr_{B,small}\right), \quad (9)$$

where *Coeff* = A, B, or C. Table 5 lists all the coefficients of Equation (9) and the goodness of fit.

It appears from Figure 4 that the A, B, and C coefficients are not independent parameters but are actually highly correlated. Specifically, A and C differ by a scale factor while B is a mirror image of A and C with a constant scale factor. This correlation is demonstrated in Figure 5.

The linear correlations of Figure 5 can be represented by Equations 10-11:

$$B = -7.88736882A - 0.19527227 \quad \left(R^2 = 1\right) \quad (10)$$

$$C = 15.55306591A + 0.75275399 \quad \left(R^2 = 0.9999\right) \quad (11)$$

Substituting Equations 10 and 11 into Equation 8 yields Equation 12:

$$\Delta r_B = A\left(a_{pc}^2 - 7.88736882a_{pc} + 15.55306591\right) - 0.19527227a_{pc} + 0.75275399, \quad (12)$$

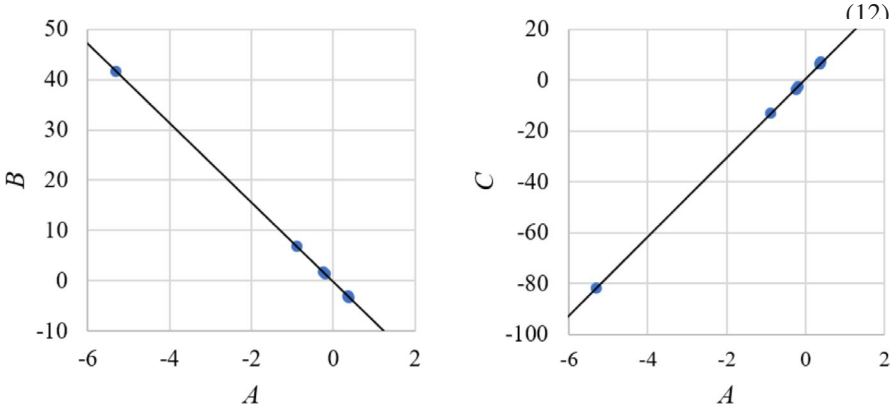

FIGURE 5 Coefficients of Equation 8 as functions of one another

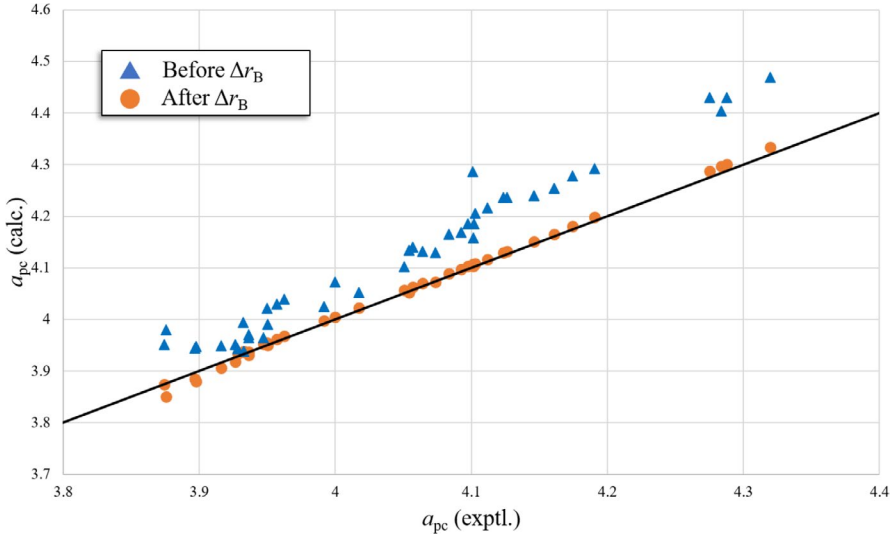

FIGURE 6 Comparison of experimental a_{pc} values to a_{pc} calculated using Equation 7. The triangles show a_{pc} before Δr_B has been applied and the circles show a_{pc} after Δr_B has been applied. The trend line represents a_{pc} (calc.) = a_{pc} (exptl.)

where a_{pc} is calculated using Equation 7. The advantage of Equation (12) is that it allows for the prediction of the B-site size correction factor, Δr_B, using only a single coefficient, A, which can be easily calculated from Equation (9) and the coefficients in Table 5 as

$$A = -0.11987 + 0.80266\tan\left(2Zr_{B,small}\right) + 1.29757\sin\left(3Zr_{B,small}\right) \quad (13)$$

Since Equation 7 was developed from perovskite data which contained random distributions of cations on both the A and B sites, it does not accurately predict a_{pc} in B-site ordered perovskites, as Table 1 and Figure 6 demonstrate. The pseudocubic lattice constant calculated from Equation 7 tends to be larger than the experimental pseudocubic lattice constant, which further demonstrates that the model overestimates the unit cell volume for B-site ordered perovskites; however, Figure 6 also shows that after the volume shrinkage resulting from B-site ordering has been accounted for, Equation 7 is still an accurate predictor of the pseudocubic lattice constant. Thus, the model as developed previously[49] has been effectively extended to account for rock salt B-site ordering.

A major implication of this model is that it can be used to accurately predict the volume shrinkage as the result of rock salt B-site ordering in perovskites; however, it should be noted that the model is only generally applicable to rock salt B-site ordered perovskites with the smallest B-site species between 0.565 (Ru^{5+}) and 0.64 (Nb^{5+}, Ta^{5+}) and ionic charges between 4+ and 6+. Although the model *may* be more generally applicable, like all empirical models, it cannot be extrapolated beyond the upper and lower bounds in the data set with any degree of certainty.

4 | CONCLUSIONS

Using a solid-state mixed-oxide method, four compositions within the $A(Zn_{0.5}Ti_{0.5})O_3$ system (A = Nd, Sm, $La_{0.5}Nd_{0.5}$, $Nd_{0.5}Gd_{0.5}$) were successfully synthesized. The XRD patterns show long-range rock salt B-site order is present within all of the compositions. Seven system-specific models were derived for the B-site size adjustment factor, Δr_B, as a function of a_{pc}. A general model for rock salt B-site ordering in perovskites, which accounts for both the charge and size of the smallest B-site species, was derived based upon these specific models. One of the major implications of this model is that it accurately predicts the volume shrinkage, and so pseudocubic lattice constant, for any $A_2(B'B'')O_6$ rock salt B-site ordered perovskites using only readily available ionic radii data. Conversely, it might be used to determine the degree of order in a given perovskite from experimental measurements of lattice constants. It may even be possible with more data to extend this model to predict volume shrinkage in other B-site ordered perovskite systems (eg, those with 1:2 ordering).

ACKNOWLEDGMENTS

This work has been supported by the Micron School of Materials Science and Engineering at Boise State University.

ORCID

Evan Smith https://orcid.org/0000-0002-1603-0517

REFERENCES

1. Miller V, Tidrow S. Perovskites: temperature and coordination dependent ionic radii. Integrated Ferroelectrics. 2013;148:1–16.
2. King G, Woodward P. Cation ordering in perovskites. J Mater Chem. 2010;20:5785–96.
3. Setter N, Cross LE. The contribution of structural disorder to diffuse phase transitions in ferroelectrics. J Mater Sci. 1980;15(10):2478–82.
4. Zhang X, Wang Q, Gu B. Study of the order-disorder transition in $A(B'B'')O_3$ perovskite type ceramics. J Am Ceram Soc. 1991;74(11):2846–50.
5. Gui H, Gu B, Zhang X. Order-disorder transition in $(A'A'')BO_3$ and $A(B'B'')O_3$ complex perovskite crystals. J Am Ceram Soc. 1996;79(2):381–4.
6. Woodward P, Hoffmann R, Sleight A. Order-disorder in $A_2M^{3+}M^{5+}O_6$ perovskites. J Mater Res. 1994;9(8):2118–27.
7. Lufaso M, Barnes P, Woodward P. Structure prediction of ordering and disordered multiple octahedral cation perovskites using SPuDS. Acta Crystallogr Sect B Struct Sci. 2006;62(3):397–410.
8. Anderson M, Greenwood K, Taylor G, Poeppelmeier K. B-cation arrangements in double perovksites. Prog Solid State Chem. 1993;22(3):197–233.
9. Howard C, Kennedy B, Woodward P. Ordered double perovskites—a group-theoretical analysis. Acta Crystallogr Sect B Struct Sci. 2003;59(4):463–71.
10. Yang JH, Choo WK, Lee CH. Ca_2MgWO_6 from neutron and X-ray powder data. Acta Crystallogr Sect C Cryst Struct Commun. 2003;59(8):i86–i88.
11. Patwe SJ, Achary SN, Mathews MD, Tyagi AK. Crystal structure and thermal expansion behavior of Ca_2MgWO_6. Mater Chem Phys. 2006;98(2–3):486–93.
12. Mishra AK, Poswal HK, Acharya SN, Tyagi AK, Sharma SM. Structure evolution of double perovskite Sr_2MgWO_6 under high pressure. Phys Status Solidi. 2010;247(7):1773–7.
13. Khalyavin DD, Senos A, Mantas PQ. Crystal structure of Sr_2MgWO_6 and Ba_2MgWO_6 determined by powder X-ray diffraction. Powder Diffr. 2004;19(03):280–3.
14. Achary SN, Chakraborty KR, Patwe SJ, Shinde AB, Krishna P, Tyagi AK. Anisotropic thermal expansion behavior in tetragonal Sr_2MgWO_6. Mater Res Bull. 2006;41(3):674–82.
15. Vasala S, Lehtimäki M, Haw SC, Chen JM, Liu RS, Yamauchi H, et al. Isovalent and aliovalent substitution effects on redox

chemistry of $Sr_2MgMoO_{6-\delta}$ SOFC-anode material. Solid State Ionics. 2010;181(15–16):754–9.
16. Patwe SJ, Achary SN, Mathews MD, Tyagi AK. Synthesis, phase transition and thermal expansion studies on M_2MgWO_6 (M=Ba^{2+} and Sr^{2+}) double perovskites. J Alloys Compd. 2005;390(1–2):100–5.
17. Bugaris DE, Hodges JP, Huq A, zur Loye H-C. Crystal growth, structures, and optical properties of the cubic double perovskites Ba_2MgWO_6 and Ba_2ZnWO_6. J Solid State Chem. 2011;184(8):2293–8.
18. Day BE, Bley ND, Jones HR, McCullough RM, Eng HW, Porter SH, et al. Structures of ordered tungsten- or molybdenum-containing quaternary perovskite oxides. J Solid State Chem. 2012;185:107–16.
19. Filip'ev VS, Shatalova GE, Fesenko EG Determination of bond lengths in tungstates with Perovskite-type structure. Kristallografiya. 1974;19(2):386–7.
20. Meenakshi S, Vijayakumar V, Achary SN, Tyagi AK. High pressure investigation on double perovskite Ba_2MgWO_6. J Phys Chem Solids. 2011;72(6):609–12.
21. Agranovskaya AI. Physical-chemical investigation of the formation of complex ferroelectrics with perovskite structure. Izv Akad Nauk SSSR, Seriya Fiz. 1960;24:1275–81.
22. Zaslavskii AI, Bryzhina MF. An X-ray structural investigation of the antiferroelectric Pb_2MgWO_6 and the system of the solid solutions Pb_2MgWO_6-$PbTiO_3$. Kristallografiya. 1962;7:709–17.
23. Baldinozzi G, Sciau P, Buffat P-A. Investigation of the orthorhombic structures of Pb_2MgWO_6 and Pb_2CoWO_6. Solid State Commun. 1993;86(9):541–4.
24. Baldinozzi G, Sciau P, Pinot M, Grebille D. Crystal structure of the antiferroelectric perovskite Pb_2MgWO_6. Acta Crystallogr Sect B Struct Sci. 1995;51(5):668–73.
25. Singh AK, Singh AK. Low temperature phase transition studies on $Pb(Mg_{0.5}W_{0.5})O_3$ ceramic. Solid State Sci. 2012;14(1):100–5.
26. Ubic R, Hu Y, Abrahams I. Neutron and electron diffraction studies of $La(Zn_{1/2}Ti_{1/2})O_3$ perovskite. Acta Crystallogr Sec B Struc Sci. 2006;62:521–9.
27. Tseng C-F, Huang C-L, Yang W-R, Hsu C-H. Dielectric characteristics of $Nd(Zn_{1/2}Ti_{1/2})O_3$ ceramics at microwave frequencies. J Am Ceram Soc. 2006;89(4):1465–70.
28. Das N, Nath M, Thakur G, Thirumal M, Ganguli A. Monoclinically distorted perovskites, A_2ZnTiO_6 (A=Pr, Gd): Rietveld refinement, and dielectric studies. J Solid State Chem. 2015;229:97–102.
29. Aguadero A, Alonso J, Martínez-Lopez M, Fernández-Díaz M. Crystallo-chemical evolution of the La_2ZnTiO_6 double perovskite upon reduction: A structural study. Solid State Sci. 2011;13:13–8.
30. Suchomel M, Fogg A, Allix M, Niu H, Claridge J, Rosseinsky M. Bi_2ZnTiO_6: A lead-free closed-shell polar perovskite with a calculated ionic polarization of 150 μC cm^{-2}. Chem Mater. 2006;18:4987–9.
31. Wakeshima M, Harada D, Hinatsu Y. Crystal structures and magnetic properties of ordered perovskites $A_2R^{3+}Ir^{5+}O_6$ (A=Sr, Ba; R=Sc, Y, La, Lu). J Alloy Compd. 1999;287:130–6.
32. Vasala S, Yamauchi H, Karppinen M. Synthesis, crystal structure and magnetic properties of a new B-site ordered double perovskite Sr_2CuIrO_6. J Solid State Chem. 2014;220:28–31.
33. Howard C, Barnes P, Kennedy B, Woodward P. Structures of the ordered double perovskites Sr_2YTaO_6 and Sr_2YNbO_6. Acta Crystallogr Sec B Struc Sci. 2005;61:258–62.
34. Zhou Q, Kennedy B, Avdeev M. Structural studies of the disorder and phase transitions in the double perovskite Sr_2YTaO_6. J Solid State Chem. 2010;183:1741–6.
35. Henmi K, Hinatsu Y, Masaki N. Crystal structures and magnetic properties of ordered perovskites Ba_2LnNbO_6 (Ln = lanthanide elements). J Solid State Chem. 1999;148:353–60.
36. Doi Y, Hinatsu Y. Manetic properties of ordered perovskites Ba_2LnTaO_6 (Ln = Y, lanthanides). J Phys: Condens Matter. 2001;13:4191-202.
37. Kanaiwa Y, Wakeshima M, Hinatsu Y. Synthesis, crystal structure, and magnetic properties of ordered perovskites Sr_2LnTaO_6 (Ln = lanthanides). Mater Res Bull. 2002;37:1825–36.
38. Ting V, Liu Y, Withers R, Norén L, James M, FitzGerald J. A structure and phase analysis investigation of the 1:1 ordered A_2InNbO_6 perovskites (A = Ca^{2+}, Sr^{2+}, Ba^{2+}). J Solid State Chem. 2006;179:551–62.
39. Vasala S, Lehtimäki M, Huang Y, Yamauchi H, Goodenough J, Karppinen M. Degree of order and redox balance in B-site ordered double-perovskite oxides, $Sr_2MMoO_{6-\delta}$ (M=Mg, Mn, Fe Co, Ni, Zn). J Solid State Chem. 2010;183:1007–12.
40. Prior T, Couper V, Battle P. Structural chemistry of the cation-ordered perovskites $Sr_2CaMo_{1-x}Te_xO_6$ ($0 \le x \le 1$). J Solid State Chem. 2005;178:153–7.
41. Goldschmidt V. The laws of crystal chemistry. Naturwissenschaften. 1926;14:477–85.
42. Shannon R. Revised effective ionic-radii and systematic studies of interatomic distances in halides and chalcogenides. Acta Crystallogr Sec A. 1976;32:751–67.
43. Ubic R. Revised method for the prediction of lattice constants in cubic and pseudocubic perovskites. J Am Ceram Soc. 2007;90(10):3326–30.
44. Ubic R, Subodh G, Sebastian M, Gout D, Proffen T. Structure of compounds in the $Sr_{1-3x/2}Ce_xTiO_3$ homologous series. Chem Mater. 2008;20:3127–233.
45. Ubic R, Subodh G, Gout D, Sebastian M, Proffen T. Crystal structure of $Sr_{0.4}Ce_{0.4}TiO_3$ ceramics. Chem Mater. 2009;21:4706–10.
46. Ubic R, Subodh G, Sebastian M, Gout D, Proffen T. Effective size of vacancies in the $Sr_{1-3x/2}Ce_xTiO_3$ superstructure. Ceram Trans. 2009;204:177–85.
47. Ubic R, Tolman K, Chan K, Lundy N, Letourneau S, Kriven W. Effective size of vanancies in aliovalently doped $SrTiO_3$ perovskites. J Alloys Compd. 2013;575:239–45.
48. Tolman KR, Ubic R, Papac M, Seymour KC, McCormack SJ, Kriven WM, et al. Structural effect of aliovalent doping in lead perovskites. J Solid State Chem. 2015;225:359–67.
49. Ubic R, Tolman K, Talley K, Joshi B, Schmidt J, Faulkner E, et al. Lattice-constant prediction and effect of vacancies in aliovalently doped perovskites. J Alloys Compd. 2015;644:982–95.
50. Smith E, Tolman K, Ubic R. An empirical model for B-site cation ordering in $Ba(Mg_{1/3}Ta_{2/3})O_3$. J Alloys Compd. 2018;735:2356–62.
51. Tolman K, Ubic R, Liu B, Williamson I, Bedke K, Nelson EB, et al. Empirical evidence for A-site order in perovskites. J Am Ceram Soc. 2017;100:429–42.
52. Smith E, Ubic R. Empirical models for layered A-site ordering in perovskite titanates. J Am Ceram Soc. 2019;102:3019–31.
53. Coomer F, Campbell J, Giordano N, Collins O, Cussen E. Structural and magnetic study of Yb^{3+} in the perovskites Sr_2TbMO_6 (M=Nb, Ta, Sb). J Solid State Chem. 2015;221:411–7.

54. Doi Y, Hinatsu Y, Oikawa K, Shimojo Y, Morii Y. Magnetic and neutron diffraction study on the ordered perovskite Sr_2HoRuO_6. J Mater Chem. 2000;10:797-800.
55. Doi Y, Hinatsu Y, Oikawa K, Shimojo Y, Morii Y. Magnetic and neutron diffraction study on ordered perovskites Sr2LnRuO6 (Ln=Tb, Ho). J Alloys Compd. 2001;4:455–9.
56. Battle P, Grey C, Hervieu M, Martin C, Moore C, Paik Y. Structural chemistry and magnetic properties of La_2LiRuO_6. J Solid State Chem. 2003;175:20–6.
57. Zhou Q, Kennedy B, Wallwork K, Elcombe M, Lee Y, Vogt T. Temperature and pressure dependent structural studies of the ordered double perovskites $Sr_2TbRu_{1-x}Ir_xO_6$. J Solid State Chem. 2005;178:2282–91.
58. Wittmann U, Rauser G, Kemmler-Sack S. Ueber die ordnung von B(III) und M(V) in perowskiten com typ A(II)2 B(III) M(V) O_6 (A(II) = Ba, Sr; M(V) = Sb, Nb, Ta). Zeitshrift fuer Anorganische und Allgemeine Chemie. 1981;482:143–53.
59. Shaheen R, Bashir J. Crystal structure of A_2InSbO_6 (A=Ca, Sr, Ba) ordered double perovskites. Solid State Sci. 2010;12:605–9.
60. Fu W, Gelder R, Graaff R. Crystal structure of the ordered perovskite: $BaBi_{0.5}Sb_{0.5}O_3$. Mater Res Bull. 1997;32(6):657–62.
61. Faik A, Igartua J, Gateshki M, Cuello G. Crystal structures and phase transitions of Sr_2CrSbO_6. J Solid State Chem. 2009;182:1717–25.
62. Lufaso M, Macquart R, Lee Y, Vogt T, Loye H. Structural studies of Sr_2GaSbO_6, and Sr_2FeNbO_6 using pressure and temperature. J Phys: Condens Matter. 2006;18:8761–80.
63. Faik A, Orobengoa D, Iturbe-Zabalo E, Igartua JM, Iturbe-Zabalo E, Igartua J. A study of the crystal structures and the phase transitions of the ordered double perovskites Sr_2ScSbO_6 and Ca_2ScSbO_6. J Solid State Chem. 2012;192:273–83.
64. Faik A, Iturbe-Zabalo E, Urcelay I, Igartua J. Crystal structures and high-temperature phase transitions of the new ordered double perovskites Sr_2SmSbO_6 and Sr_2LaSbO_6. J Solid State Chem. 2009;182:2656–63.
65. Fu W, IJdo D. On the structure of $BaTl_{0.}5S_{b0.5}O_3$: an ordered perovskite. J Solid State Chem. 1997;128:323–5.

How to cite this article: Smith E, Adams C, Ubic R. Correlative models for perovskites with rock salt B-site ordering. *J Am Ceram Soc*. 2019;00:1–12. https://doi.org/10.1111/jace.16695